ADVANCED FUNCTIONAL MATERIALS
www.afm-journal.de

Red–Green–Blue Light Emission from Composition Tunable Semiconductor Micro-Tripods

Xiaohang Song, Zitong Xu, Bo Gao, Xuyang Li, Qihang Lv, Rui Zhang, Bingjie Wang, Hulin Zhang, Pengfei Guo,* and Johnny C. Ho*

Micro/nanoscale lasers that span the entire visible spectrum, especially those in red, green, and blue colors, are not only essential for a variety of optical devices but also have important applications in visible color communication, multi-color fluorescence sensing, and wavelength division multiplexing. Despite the great efforts made to achieve multi-color lasing using a variety of approaches, on-chip white light emission and even red, green, and blue multi-color lasers still suffer from considerable challenges in micro-nano structures. Here, CdS_xSe_{1-x}, CdS, and ZnS micro-tripod structures are successfully prepared using chemical vapor deposition approaches. The micro-photoluminescence (μ-PL) spectra and PL-mapping of these micro-tripods reveal various emissions at 630, 508, and 460 nm, respectively. Additionally, white-light emissions based on these composition-tunable tripods are realized through an end-coupling structure system. Moreover, room-temperature modes tunable lasers are observed clearly from three legs of these micro-tripods, with a low threshold of ≈48.39 μJ cm^{-2} and a high quality factor of 1227.3. The realization of micro-tripods-based lasers may provide an innovative way for highly integrated photonic circuits and communications.

1. Introduction

In recent years, semiconductor materials with controllable bandgaps have become a flourishing research field due to their unique properties, rendering them promising candidates for various applications.[1–5] Especially, semiconductor-based solid-state white-light emitters have attracted tremendous attention for their higher conversion efficiency than conventional incandescent lamps.[6–10] Generally, two effective approaches exist for the realization of white-light sources based on the semiconductor materials. The first one is synthesizing semiconductor alloys with controllable bandgaps,[11–13] and the second one is the artificially constructed white-light emitters by various semiconductors with high-efficiency monochromatic emissions.[6,14–16] However, solid-state white-lighting devices generated from red–green–blue emitters based on semiconductor structures or photonic systems are still challenging in the photonic research.[1,2,17] For instance, a suitable mix for white-light radiation with favorable wavelengths and intensity ratios, proper color rendering index, and high stability is still lacking.[18,19] In particular, a white laser, with high Q factor and low threshold simultaneously is quite challenging and is an urgent issue to be solved, owing to the energy loss from the light transmission process, reflection energy loss from the cavities, and energy loss from the cavities coupling of the gain materials.[17,20]

The emerging nanoscience and technology have brought inspiration and provided a variety of opportunities for colorful light emitters with tunable ability and high quantum efficiency.[4,21–27] Particularly, low-dimensional semiconductor nanostructures, such as nanowires, nanoplates, and nanoribbons, can be synthesized by applying an in situ concentration changing system of the source materials during the growth process.[2,28,29] For example, all-inorganic $CsPbX_3$ (X = Cl, Br, I) perovskites nanocrystals or wires have been reported to realize the wavelength tunable lasers ranging from 412 to 700 nm, which almost covers the entire visible region.[22,30,31] The compositions of CdS_xSe_{1-x} nanowires or nanoribbons have been reported to be fabricated along a single substrate or single nanostructures through a source moving chemical-vapor-deposition (CVD) method, which is used to construct the broad wavelength tunable lasers[3,32,33] or multi-wavelength lasers.[1,2,17,34] The composition gradient $In_xGa_{1-x}N$ nanowires have been reported to grow via a CVD method on a single substrate, which exhibits a continuous PL emission ranging from 325 to 850 nm with increasing indium

X. Song, Z. Xu, X. Li, Q. Lv, B. Wang, H. Zhang, P. Guo
College of Electronic Information and Optical Engineering
Taiyuan University of Technology
Taiyuan 030024, China
E-mail: guopengfei@tyut.edu.cn
B. Gao
Instrumental Analysis Center
Taiyuan University of Science and Technology
Taiyuan 030024, China
R. Zhang
Department of Physics
Taiyuan University of Science and Technology
Taiyuan 030024, China
E-mail: zrzx_0921@tyust.edu.cn
P. Guo, J. C. Ho
Department of Materials Science and Engineering
City University of Hong Kong
Kowloon, Hong Kong 999077, China
The ORCID identification number(s) for the author(s) of this article can be found under https://doi.org/10.1002/adfm.202403135

DOI: 10.1002/adfm.202403135

concentration x.[35] The $Cd_xPb_{1-x}S$ alloy nanowires and heterostructures were conveniently created through a single-step CVD growth process, which shows simultaneous emission in mid-infrared and visible wavelengths.[36] Besides these examples of wavelength-tunable emitters and lasers based on the composition-graded structures, modes tunable oscillations based on the absorption-emission-absorption process were also reported based on the group II–VI semiconductor wires.[37,38] Despite all this extraordinary progress, the generation of room-temperature multi-color semiconductor light emitters and artificial multifunctional resonators, which cover the full visible spectrum with low energy loss, are urgently needed for digital communications and full-color displays.[2,5,39]

Although wavelength-tunable emitters with gradient gain materials and resonant cavities have been realized using different semiconductor micro/nanostructures, red–green–blue emitters based on the composition graded micro-tripods, to the best of our knowledge, have never been reported. In this work, we report a sample CVD approach to achieve room-temperature red–green–blue emitters and microscale mode-tunable lasers based on various components of micro-tripods. The scanning electron microscopy (SEM), energy dispersive X-ray spectroscopy (EDX), and transmission electron microscopy (TEM) characterizations results prove that these tripods have high crystalline with three legs angle to each other about 120°. The PL emissions and 2D PL mapping investigations indicate that these tripod structures have uniform light emissions with wavelength peaks at 460 nm, 508 nm, and 630 nm, respectively. Additionally, artificially coupled white-light emitters with broad PL emissions using the ZnS, CdS, and CdSSe micro-tripods are successfully realized. Moreover, high-quality mode-tunable lasers have been achieved based on these micro-tripods under pulsed laser excitation at room temperature. These novel micro-scale lasers with tripod cavities not only provided a mode-tunable lasing, but also gave a potential materials platform for wavelength continuous tunable lasers based on the bandgap gradient CdS_xSe_{1-x} tripod structures. A flexible artificial manipulation method is used to fabricate the white-light emitters based on these bandgap tunable tripods, providing an excellent platform for the fabrication of on-chip solid-light sources and full-color displays. All these results represent a significant step toward high-integration optical circuits and photonics communications in the future.

2. Results and Discussion

These ZnS nanostructures are synthesized via a CVD method, as shown in Figure S1 (Supporting Information) and Experiment Sections. These micro-tripods structures are grown through a self-assembled mechanism. As an example, a proposed schematic growth process of a typical micro-tripod is shown in Figure S2 (Supporting Information). Top-view low- and high-resolution scanning electron microscopy (SEM) images (**Figure** 1a–d) reveal that the as-grown structures are micro-tripods, which have three legs of 1–2 µm in length and 80–100 nm in diameter. The angles between each branch (leg) are 117°, 123°, and 120°, respectively, as shown in Figure 1d. Side-view SEM images (Figure 1e; Figure S3, Supporting Information) of a typical micro-tripod show that the tripod's three legs grow diagonally upward on the silicon substrate without any intermediate structures and buffer layers. Figure S4 (Supporting Information) shows the SEM image of the initial growth stage of the micro-tripods. As we can see, the seed structures of the micro-tripods grow directly on the substrate, where the branches begin to appear. Figure 1f and Figure S5 (Supporting Information) show the EDX spectra of the ZnS micro-tripods, which show the atomic ratio of Zn and S is close to 1:1 with negligible Sn. In order to clearly show the element distribution of the Sn-doped ZnS tripods, a selected typical ZnS tripod (Figure 1g) and 2D element mapping (Figure 1h–j) of the tripod are investigated. It can be observed that the two detected elements, Zn and S, are evenly distributed along the entire tripod structure, while the Sn element is not obviously observed due to its lower content. Figure 1k shows these tripods' X-ray diffraction (XRD) patterns ranging from 20° to 55°. The sharp diffraction peaks confirm that these ZnS tripods have excellent crystalline indexed to the cubic structures and show good agreement with the XRD Card (JCPDS: 05–0566) for powder ZnS. The standard card information of the XRD profiles is shown in Figure S6 (See Supporting Information)

In order to realize the red–green–blue tri-color emissions, CdS and CdS_xSe_{1-x} tripods are also investigated besides the ZnS tripods, as shown in **Figure 2**. The high-resolution top-view SEM image and 2D element mapping of Sn-doped CdS micro-tripod are shown in Figure 2a–d, respectively, which shows that Cd, S, and Sn are uniformly distributed along the three branches. Figure S7 (Supporting Information) shows the EDX spectrum of a typical CdS tripod; the atomic ratio of Cd and S is close to 1:1, with negligible Sn (2.31%) in the tripod structure. The XRD pattern of these CdS tripods is shown in Figure 2e, which is indexed to the hexagonal wurtzite phase and matched with the PDF card (No: 41–1049). Figure 2f–j shows the top-view SEM image and 2D element mapping of a typical Sn-doped CdS_xSe_{1-x} micro-tripod on the Si substrate. It can be seen that Cd, S, Se, and Sn are uniformly distributed along the three branches of the tripod, and the atomic ratio is about 47.42:24.54:26.53:1.51 according to the EDX spectra in Figure S8 (Supporting Information). In general, it is known that the bandgap of a ternary alloy is determined by an interpolation between those of the two binaries with additional nonlinear bending for CdS_xSe_{1-x} and the bandgap bowing coefficient (b = 0.54). Using the alloy composition determined by EDX as shown in Figure S8 (Supporting Information), we can obtain the bandgap of the mole fraction of this CdS_xSe_{1-x} tripod by using the following equation[40,41]:

$$E_g\left(CdS_xSe_{1-x}\right) = xE_g(CdS) + (1-x)E_g(CdSe) - x(1-x)b \quad (1)$$

The wavelength is calculated as follows[42]:

$$E_g = hc/\lambda \quad (2)$$

By calculation, there is a good agreement between the PL emission and the bandgap of the alloy CdS_xSe_{1-x} (x = 0.48).

Figure 2k shows the XRD pattern of the $CdS_{0.48}Se_{0.52}$ alloy micro-tripods, which is indexed to the hexagonal wurtzite structure and offers a reasonable consistency with pure CdSe (JCPDS: 08–0459) and CdS (JCPDS: 41–1049) in Figure 2k, respectively. For example, a typical $CdS_{0.48}Se_{0.52}$ alloy micro-tripod is selected and placed on a microgrid for structural characterization by transmission electron microscopy (TEM) (see Figure S9, Supporting

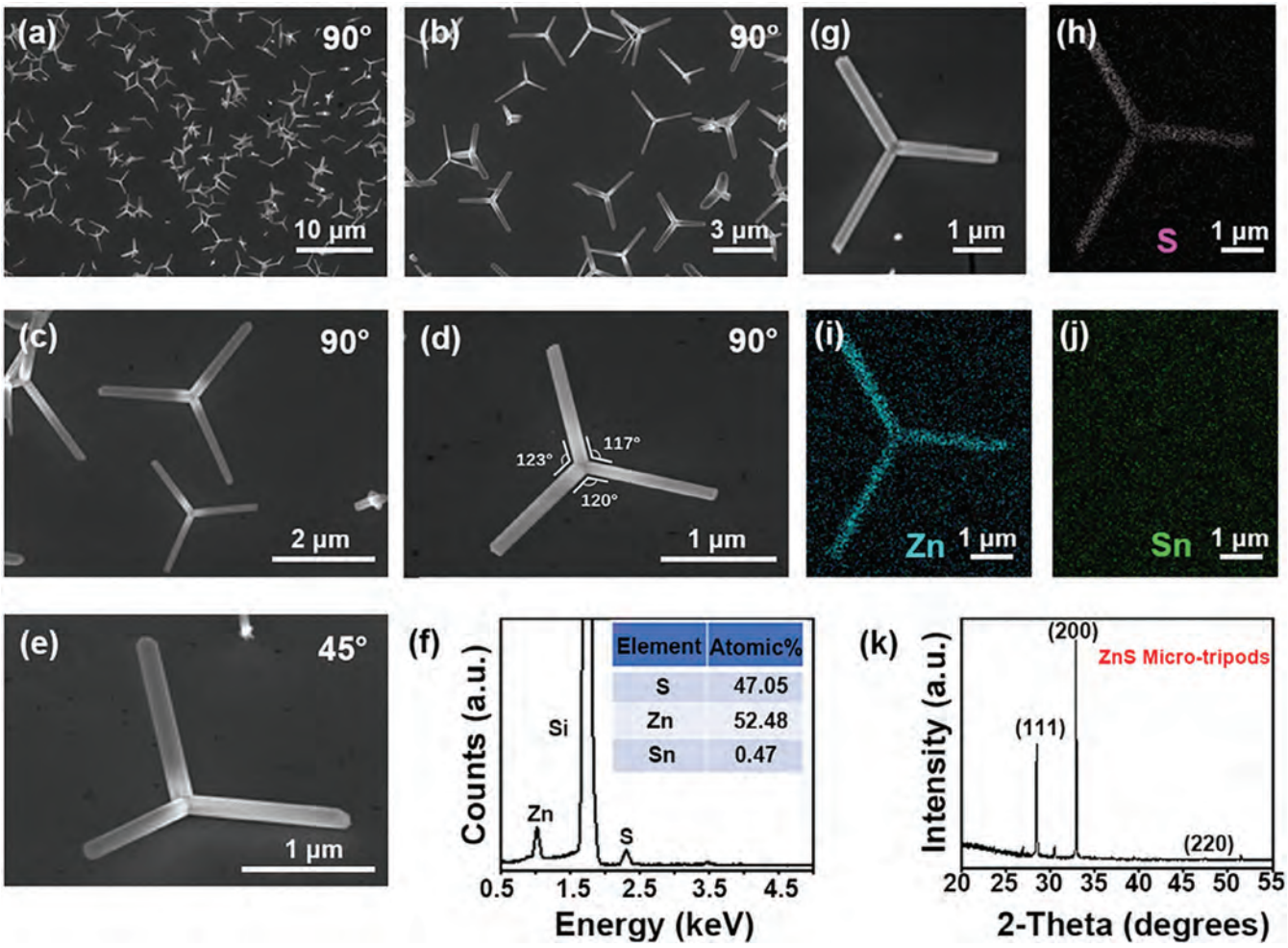

Figure 1. Structural characterization of ZnS micro-tripods. a,b) Top-view (shooting angle is 90°) low-resolution SEM images of ZnS micro-tripods. c,d) Top-view high-resolution SEM images of the ZnS micro-tripods. The angles between the three branches are about 120°. e) Side-view (shooting angle is 45°) SEM image of a typical ZnS tripod on the Si substrate. f) EDX spectra of typical ZnS micro-tripods. g–j) SEM image and 2D element map of a ZnS tripod, respectively. k) The XRD pattern of the typical ZnS micro-tripod structures.

Information). Figure 2l shows a low-resolution TEM image of a $CdS_{0.48}Se_{0.52}$ tripod, indicating that three legs have a smooth surface with two branches of about 120° each. High-resolution TEM (HR-TEM) images at two typical positions from the tripod (blue and red squares as indicated in Figure 2l) are shown in Figure 2m,n, respectively. The lattice spacing of the alloy tripod can be calculated by the interplanar spacing formula for the hexagonal crystal system based on the HR-TEM image of $Cd_{0.48}Se_{0.52}$:

$$1/d^2_{hkl} = 4\left(h^2 + hk + k^2\right)/3a^2 + l^2/c^2 \quad (3)$$

where d is the interplanar spacing and a and c are the corresponding lattice constants. The lattice constant of the $CdS_{0.48}Se_{0.52}$ tripod can be approximated by Vegard's law and EDX values:

$$C_{(Cds_xse_{1-x})} = x\,(CdS) + (1-x)\,(CdSe) \quad (4)$$

It can be seen from the above formula that d_{002} = 0.343 nm, which shows good agreement with the experimental results in Figure 2m,n. The corresponding selected area electron diffraction (SAED) pattern (inset in Figure 2n) indicates that the tripod is a high-quality single-crystal wurtzite structure, and the three branches grow along the [001] direction without obvious defects and phase segregation.

The optical properties of the composition tunable micro-tripods are shown in **Figure 3**. Top-view optical photograph and dark-field real-color images of a typical ZnS tripod are shown in Figure 3a–d, respectively, excited by a 375 nm continuous wavelength (CW) laser using a self-made confocal optical microscope system (see Figure S10, Supporting Information). 2D PL emission mapping (Figure 3e) of the ZnS micro-tripod shows a uniform emission image at 460 nm. Figure 3f–h shows the corresponding PL emission spectra of three typical positions (P_1–P_3) from the ZnS tripod, which have emission peaks centered at 460 nm.

Figure 3i,l shows the optical and dark-field real-color images of CdS and $CdS_{0.48}Se_{0.52}$ tripods, respectively, showing green and red emissions under a 375 nm laser illumination. In addition,

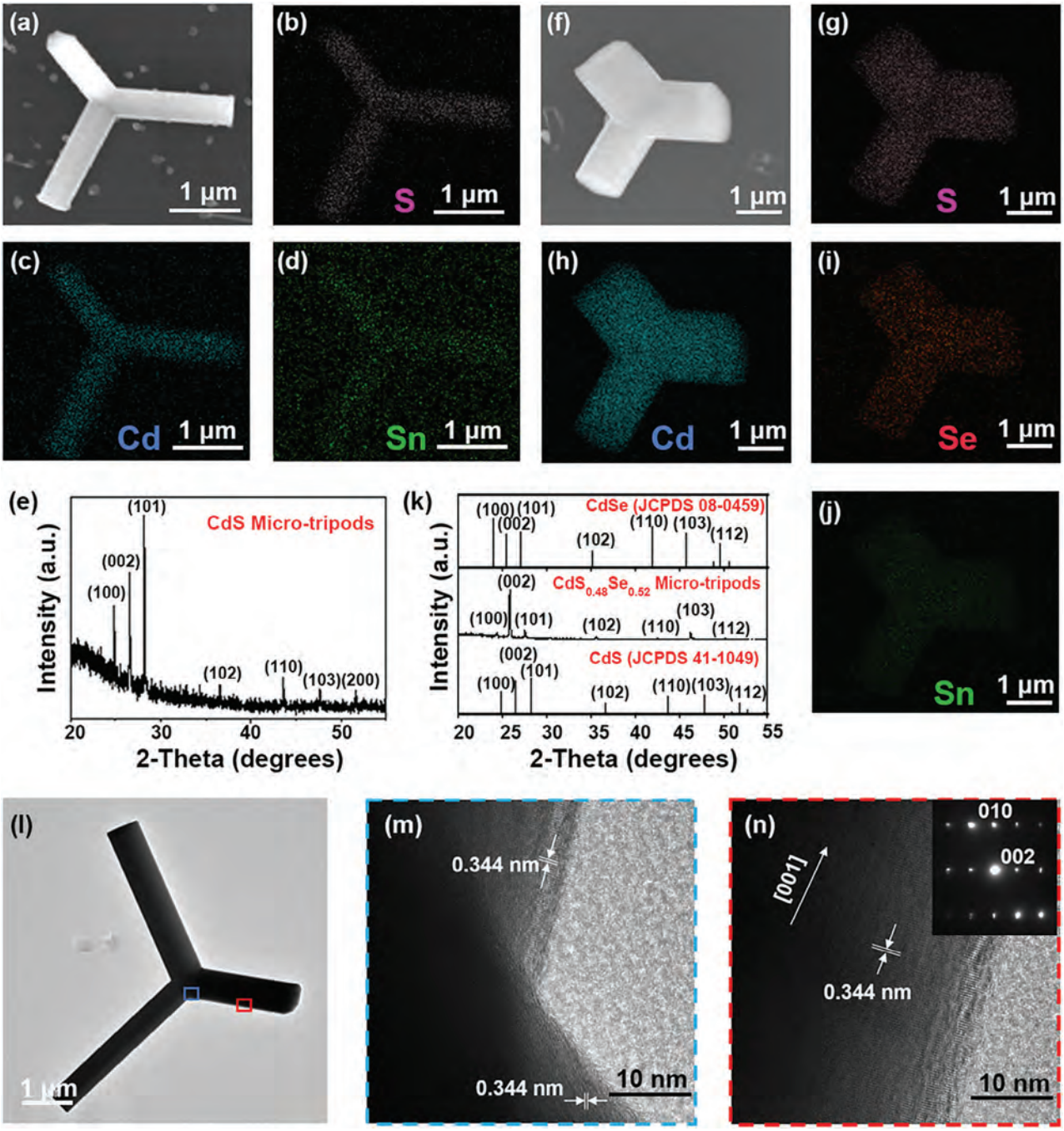

Figure 2. Structural characterization of CdS and $CdS_{0.48}Se_{0.52}$ micro-tripods. a–d) Low-resolution SEM image and 2D element mapping of CdS micro-tripods. e) The XRD pattern of CdS micro-tripods. f–j) SEM image and 2D map of $CdS_{0.48}Se_{0.52}$ micro-tripod. k) The XRD pattern of the $CdS_{0.48}Se_{0.52}$ tripods. l) Low-resolution TEM image and m,n) high-resolution TEM (HR-TEM) images of a typical $CdS_{0.48}Se_{0.52}$ micro-tripod. Inset is the corresponding SAED pattern of the tripod, as indicated in (l).

the optical waveguiding effect can be observed from the tripods' three legs, indicating that these tripods can act as good light resonators. Figure 3j,k,m,n shows 2D PL mappings and PL spectra of CdS and $CdS_{0.48}Se_{0.52}$ tripods, which shows that the tripods have uniform emissions at 508 and 629 nm, respectively, with negligible defect state emissions. All these results lay a foundation for the realization of integrated white-light emissions.

White-light sources have been a very attractive topic recently. A white-light-emitting device is proposed on a Si substrate to further illustrate the red–green–blue emissions based on these composition tunable micro-tripods. **Figure** 4a–i shows the optical photographs and dark-field images of $CdS_{0.48}Se_{0.52}$, CdS, and ZnS tripods, respectively, which show red (Figure 4b), green (Figure 4e) and blue (Figure 4f) emissions at the wavelength of

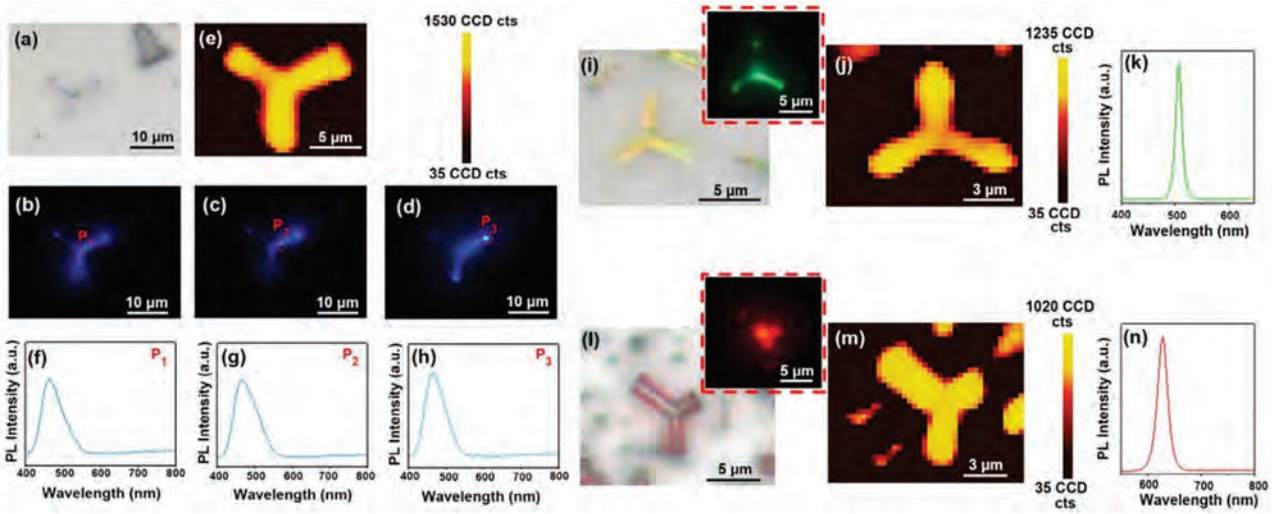

Figure 3. Optical characterization of the composition-tunable micro-tripods. a) Optical photograph of a typical ZnS micro-tripod. b–d) Dark-field real-color images of the ZnS micro-tripod excited by a 375 nm laser at three typical positions (P_1–P_3). e) 2D PL-mapping of the selected ZnS micro-tripod. f–h) Corresponding PL spectra from three positions (P_1–P_3), as indicated in (b–d), respectively. i,l) Optical photographs and dark-field images (insets) of CdS and $CdS_{0.48}Se_{0.52}$ micro-tripods under an unfocused 375 nm laser illumination. j,m) 2D PL-mapping and k,n) PL spectra of the CdS and $CdS_{0.48}Se_{0.52}$ micro-tripods, respectively.

about 630, 508, and 460 nm at room temperature with full width at half maximum (FWHM) of about 26.5, 14.1, and 30.4 nm, respectively. Figure 4j depicts a schematic diagram of the experimental configuration for the red, green, and blue tripods coupled with white-light emission. Figure S11 (Supporting Information) depicts the optical transfer process for constructing coupled composition-graded micro-tripods by a self-made optical fiber probe. As shown in Figure 4j, the spectrometer detects the optical signals, and the far-field emission image is recorded by a color camera of the charge-coupled device (CCD). Figure 4k shows the PL spectrum (T_1–T_3) of the various coupled micro-tripods system and the corresponding CIE image performed according to the PL emission spectra. A white-light emission spectrum with three typical emission peaks is centered at 630, 508, and 460 nm at room temperature, recorded at the coupling part of the micro-tripods system. The chromaticity coordinates of samples T_1–T_3 are located at the center of the white-area in the CIE diagram, which confirms that the micro-tripods coupling system can give pure white-light emission. In addition, as an example, the photothermal stability and solvent stability of the $CdS_{0.48}Se_{0.52}$ micro-tripods are investigated and shown in Figures S12 and S13 (Supporting Information), respectively. These micro-tripods structures exhibit reasonable photothermal stability and solvent stability in our work.

Based on the structural and optical characterizations of the micro-tripods, these unique micro-tripod structures may act as excellent optical confinement cavities and optical gain materials for microscale lasers.[43,44] To prove this point, stimulated emissions experiments were performed using these $CdS_{0.48}Se_{0.52}$ alloy micro-tripods by a 355 nm pulse laser excitation at room temperature (**Figure 5**). A schematic diagram of the optical setup is shown in Figure 5a. A low-resolution dark-field emission image of the tripod structures under a 355 nm laser illumination is shown in Figure 5b, in which these alloy tripods have bright red emissions at room temperature. Figure 5c,d shows the optical photograph and emission image of a typical alloy tripod, which exhibits three bright emissions guided from the tripod legs (P_1–P_3 in Figure 5d). The length of three tripod legs is about 2.2, 3.4, and 3.4 μm, as indicated in Figure 5c. Because the angle between the tripod leg and the substrate is ≈20° (Figure S14, Supporting Information), the actual length of the micro-tripod is approximately equal to the projected length in this work. Figure 5e–g shows the pumping power-dependent PL spectra and corresponding dark-field emission images (inset images) from the three legs of the micro-tripod (P_1–P_3 in Figure 5c) under a 355 nm pulse laser excitation. At the low pumping power density (34.54, 35.32, and 33.67 μJ cm^{-2}), a broad emission peak centered at ≈632 nm is recorded from the end of the tripods (P_1–P_3), which owing to a spontaneous emissions. When the pumping power increased beyond the threshold (49.77, 56.96, and 48.39 μJ cm^{-2}), sharp emission lines taking place from the tripods at the wavelengths of 641.70, 641.28, and 641.49 nm, respectively, indicating that the stimulated emissions started to occur at the tripod structures. While the power density is increased to 120 μJ cm^{-2}, the micro-tripod lasing with emission peaks at 643.38, 641.28, and 641.49 nm takes place at the three legs of tripods, respectively. Figure 5h plots the relationship between the emission intensity and the pumping power density at the three legs of a tripod. When the power density exceeds the laser threshold, the intensity of the emission line increases super-linearly, confirming the transition of the tripod from spontaneous emission to stimulated emission. Here, we have compared these micro-tripod lasers with some 1D micro- or nano-cavity lasers, as shown in **Table 1**, the lasing emissions from micro-tripods suggest the attractive oscillation cavities with high Q factors and low threshold relatively.

It is well known that due to the energy loss of photon oscillations in a resonator, the energy attenuation causes the emission redshift.[58] In addition, due to the choice of oscillation mode of the resonator, a small redshift (42–51 meV) is observed in the lasing emission peaks in Figure 5i. Figure S15 (Supporting

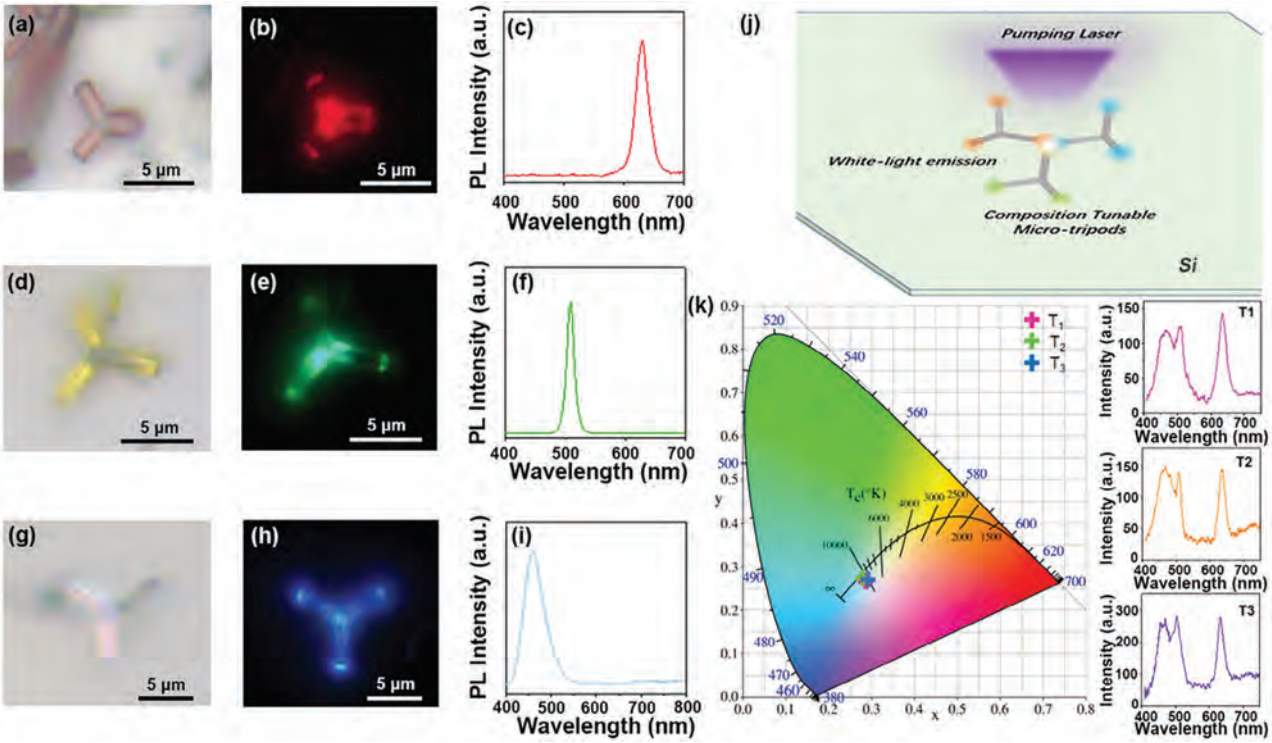

Figure 4. Red–green–blue emissions of the composition tunable micro-tripods. a,d,g) Optical photographs and b,e,h) dark-field real-color images of the typical CdS0.48Se0.52, CdS, and ZnS micro-tripods, respectively. c,f,i) Corresponding PL spectra of CdS0.48Se0.52, CdS, and ZnS micro-tripods, respectively. j) Schematic diagram of the coupled micro-tripods for white-light emission. k) PL spectrum (T1–T3) of the various coupled micro-tripods system and corresponding CIE image performed according to the PL emission spectra.

Information) shows a theoretical oscillation model, which can be considered to be a Febry–Pérot (F–P) resonator and the stimulated emission wavelength can be calculated by the following equation:

$$\lambda = 2nL/k \tag{5}$$

where n is the refractive index of the alloy tripod, L ($L = 1/2[(L_1 + L_2) + (L_2 + L_3) + (L_3 + L_1)] = L_1 + L_2 + L_3$) is the total equivalent cavity length of the tripod, and k is an integer. These results further indicate that a high-quality F–P optical cavity is formed in the tripod structure.

The quality factor (Q) of stimulated emission can be calculated by the following expression:

$$Q = \lambda/\delta\lambda \tag{6}$$

where λ is the wavelength of the stimulated emission peak and $\delta\lambda$ is the FWHM of the mode. Figure 5j shows the Q factor as a function of $1/I_x$ (x = 1,2,3, the length of each leg). After examining a dozen of other tripods, the optimized FWHM of lasing peaks ($\delta\lambda$) is about 0.52 nm, as shown in Figure S16 (Supporting Information), which shows a calculated Q factor of about 1227.3 for the tripod laser. Moreover, the lasing oscillations are also investigated and demonstrated for various micro-tripods with different sizes with equivalent cavity lengths L from 6.5 to 15.0 μm, as shown in **Figure** 6a–f. Optical photographs and dark-field emission images of six representative $CdS_{0.48}Se_{0.52}$ alloy micro-tripods with different sizes are shown in Figure 6a–f. To elucidate the influence of stimulated properties of size-dependent micro-tripods, extensive measurements of $CdS_{0.48}Se_{0.52}$ micro-tripods were performed (Figure 6). The corresponding room-temperature PL emission spectra are shown in Figure 6g, which shows wavelength continuous tunable lasing from 638.55 to 649.45 nm by the increased cavity length L ranging from 6.5 to 15.0 μm. Figure 6h shows the functional relationship between these tripods' equivalent cavity length and emission wavelength. It can be observed that the lasing peaks have a maximum redshift of about 40 meV with increasing the cavity length to 15 μm, which is due to the optical self-absorption of the Urbach tail states along the light transmission process.[41] All these results indicate that these alloy micro-tripods are excellent candidates for the manufacture of mode tunable micro-scale lasers.

Additionally, high-quality lasers with multi-color emissions at room temperature play an important role in full-color displays, white-light sources, and optical communications.[59–64] In Figure S17 (Supporting Information), lasing emissions at about 517 nm with high Q factors are also performed based on the CdS tripods in this work. Size-dependent lasing emissions of some different CdS micro-tripods structures are shown in Figure S18 (Supporting Information), which indicates that the lasing mode wavelengths of these tripods structures can also be modulated from 511.7 to 521.4 nm by the variation of structure sizes. However, because the optical properties of ZnS structures are highly sensitive to synthesis conditions, crystal size, and shapes, there are inherent defects such as vacancy and defects,[65,66] and the

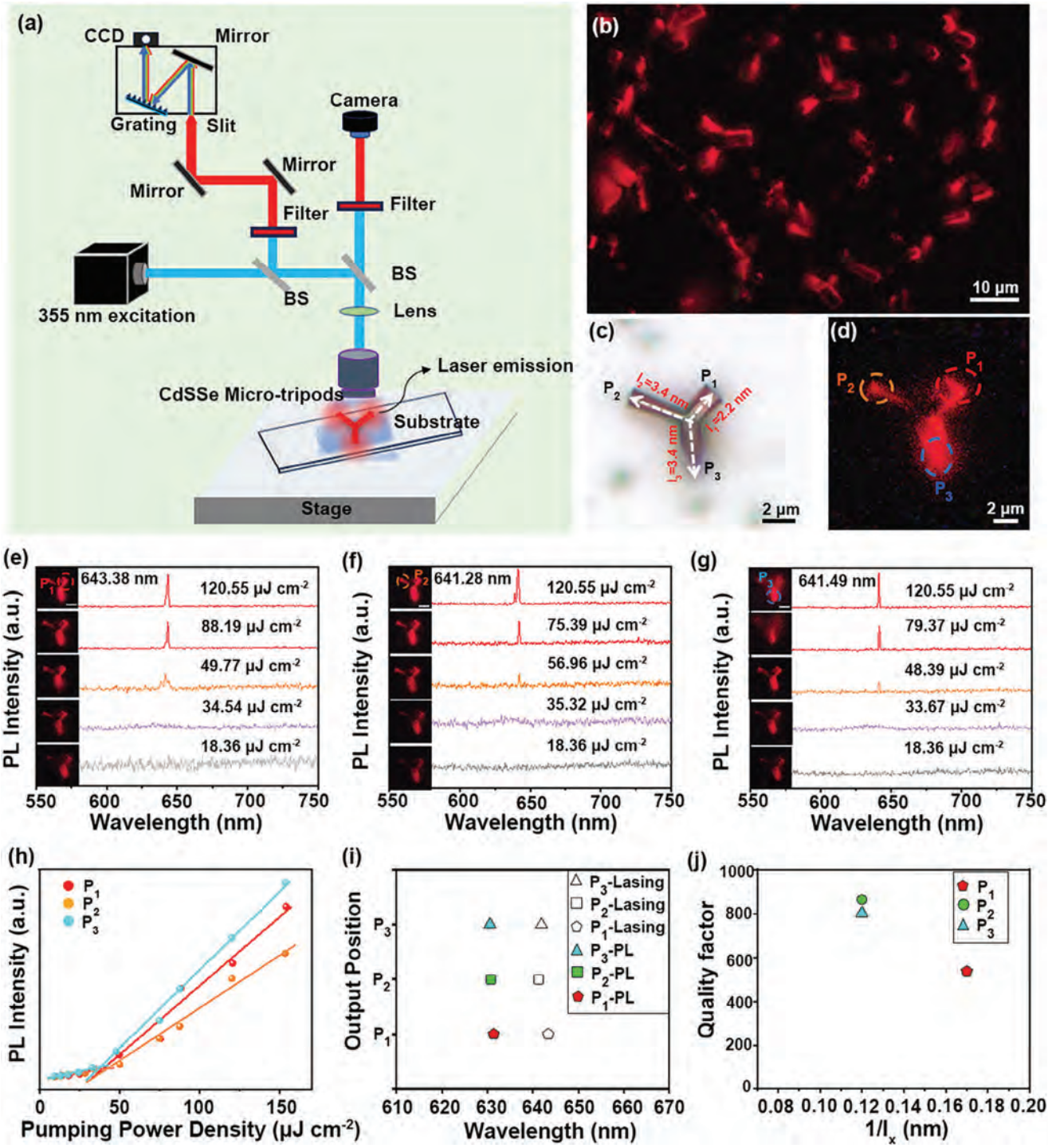

Figure 5. Stimulated emissions of Sn-doped CdS_xSe_{1-x} micro-tripods at room temperature. a) Schematic illustration of the optical setup for micro-tripods. A 355 nm pulsed laser is used for the excitation. b) Dark-field real-color image of some micro-tripods under a 355 nm pulsed laser illumination. c) Optical photograph and d) dark-field image of a typical $CdS_{0.48}Se_{0.52}$ tripod. e–j) Room-temperature pumping power-dependent PL spectra from three legs (P_1–P_3) of a single $CdS_{0.48}Se_{0.52}$ micro-tripod as indicated in (c), respectively. Insets: dark-field emission images corresponding to different pumping intensities. Scale bars are 2 μm. (h) Power-dependent emission intensity from three legs (P_1–P_3) of a micro-tripod. (i) PL emission and (j) quality factors Q from the three legs (P_1–P_3) of the micro-tripod. Here l_x means the length of different legs.

Table 1. Comparison of various structure based nano/microscale lasers.

	Sample Composition	Structure	Year	Resonator	Wavelength [nm]	Q factor	Threshold	Refs.
II–VI semiconductors	$CdS_{0.48}Se_{0.52}$	Micro-tripods	2024	F–P	641	1227.3	48.39 μJ cm^{-2}	This work
	CdS	Nanowire	2024	FP-WGM	517	>3000	50 kW cm^{-2}	[45]
	CdSe/CdSeS	Core/alloyed-crown	2023	DFB	505–535	800–1200	9–90 μJ cm^{-2}	[46]
	ZnCdSe、ZnSe、ZnS、ZnCdS	Colloidal quantum dot	2022	WGM	617, 511441	2413	22, 62, 70 μJ cm^{-2}	[47]
	CdS	Nanoribbons	2021	F–P	507.84–515.25	1051–1700	385.42 μJ cm^{-2}	[48]
	CdSe、$Cd_xZn_{1-x}S$	Composition graded QDs films	2018	Random	575, 618	–	13.7, 4.4 μJ cm^{-2}	[49]
	CdS-CdSSe-CdS	H-nanowires	2017	F–P	516, 598	1500	80 μJ cm^{-2}	[39]
	CdS_xSe_{1-x}	Composition graded nanoribbons	2016	F–P	519, 557, 623	890	3420 μJ cm^{-2}	[17]
	ZnCdSSe	Nanosheets	2015	F–P	484, 530, 642, 675	260–340	3.3 μJ cm^{-2}	[1]
	CdS_xSe_{1-x}	Composition graded nanowires	2014	F–P	517–636	–	70 μJ cm^{-2}	[32]
	CdS	Nanowire	2013	F–P	495–516	–	0.76 μJ cm^{-2}	[38]
	CdS_xSe_{1-x}	Composition graded nanowires	2013	F–P	530, 637	585	78 μJ cm^{-2}	[50]
	CdS-CdSSe-CdS	H-nanoribbon	2012	F–P	517, 583–646	920	80 kW cm^{-2}	[34]
	CdSe/CdS	Core/crown	2012	VCSEL	535	–	4.48 mJ cm^{-2}	[51]
	CdSe、CdS、ZnO	NWs on tapered fiber	2009	F–P	391, 519, 743	560–1303	1.3 μJ cm^{-2}	[14]
	CdSSe	Nanowire	2009	F–P	503–692	200	2520 μJ cm^{-2}	[52]
III–V semiconductors	InP	Micro-Ring	2021	WGM	891	–	50 μJ cm^{-2}	[53]
	InAs	Nanowire	2019	F–P	≈2500	520	50 μJ cm^{-2}	[54]
	InP/InAs	H-nanowires	2019	F–P	1573	–	2.15 mJ cm^{-2}	[55]
	AlGaAs/GaAs	H-nanowires	2017	–	781	2000	600 W cm^{-2}	[56]
	GaAs/AlGaAs	Nanowire	2016	F–P	791, 819	–	110 μJ cm^{-2}	[57]

stimulated emissions with ZnS tripods are not achieved presently. The successful preparation of red and green lasing emissions based on these CdS and CdS_xSe_{1-x} micro-tripods provides a new idea for realizing ultra-compact photonic devices.

3. Conclusion

In summary, high-quality various components micro-tripods are synthesized using a sample CVD method. Structural characterizations indicate that these micro-tripod structures have single crystalline. Red–green–blue emissions are realized based on these artificially coupled $CdS_{0.48}Se_{0.52}$, CdS, and ZnS micro-tripods systems, laying the foundation for integrating white-light sources on the chip. Moreover, room-temperature optically pumped mode-tunable microscale lasers are achieved based on these unique micro-tripod structures with a low threshold of ≈48.39 μJ cm^{-2} and a high-quality factor of 1227.3. These novel micro-scale tripod cavities represent a significant advantage in the controllable synthesis of bandgap tunable micro-tripod structures and microscale lasers, which may provide new opportunities for multi-color lasers, on-chip white-light integration, solid-state light sources, and full-color displays in the future. The theoretical oscillation model of the micro-tripod F–P cavity may open an door for the design of high-performance multi-source emitters in nanophotonics devices.

4. Experimental Section

Materials and Methods: ZnS, CdS, and CdS_xSe_{1-x} micro-tripods were grown via a conventional CVD method, as schematically shown in Figure S1 (Supporting Information). A tube furnace (OTF-1200X) was used to fabricate the tripod structures with a 2-inch quartz tube (inner diameter 45 mm, length 180 cm). First, two alumina boats with CdS powder (Alfa Aesar, 99.999%, 0.1 g) and Sn powder (Alfa Aesar, 99.999%, 0.015 g) were placed in the center and upstream of the heating zone, respectively. Several pieces of Si (4 mm × 10 mm) substrates were placed at the deposition area to collect the structures. Before heating the furnace, N_2 gas was introduced into the system at a flow rate of 100 sccm for 20 min to

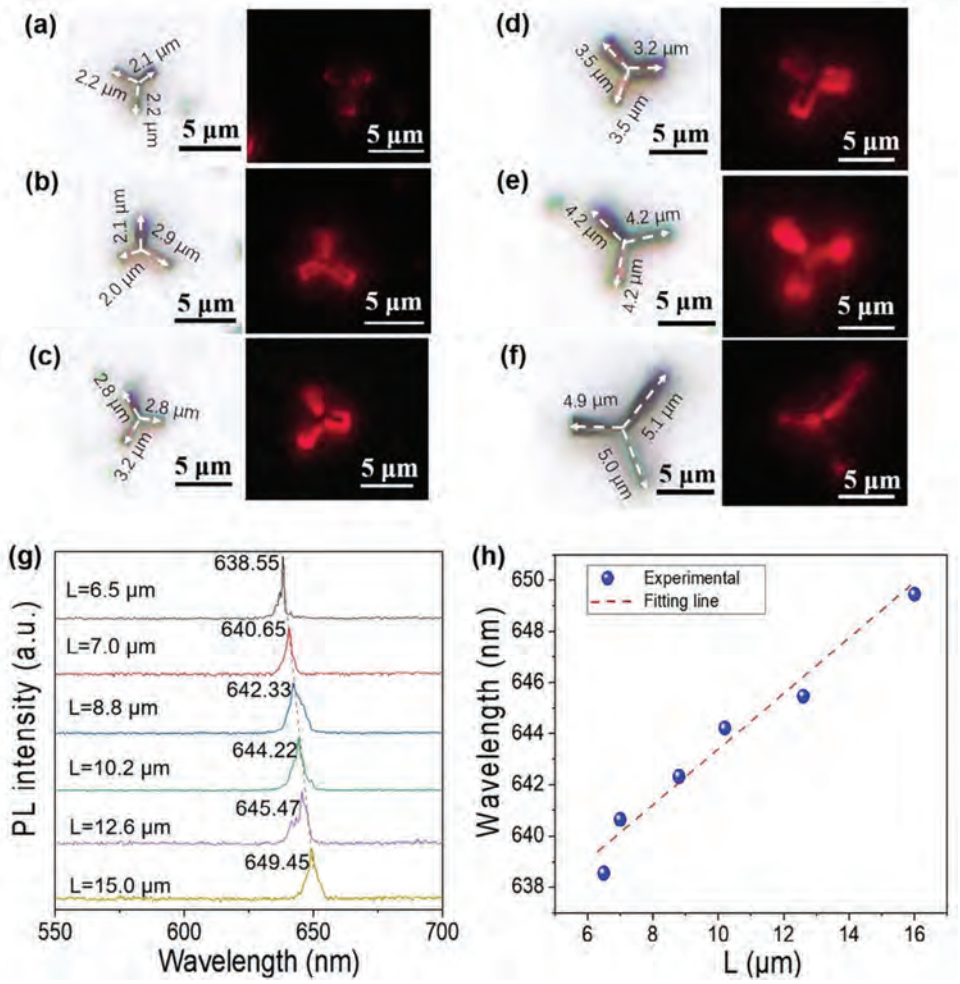

Figure 6. Room-temperature size-dependent lasing emissions of $CdS_{0.48}Se_{0.52}$ micro-tripods. a–f) Optical photographs and corresponding dark-field real-color images of $CdS_{0.48}Se_{0.52}$ micro-tripods with various sizes. g) Size-dependent lasing emissions of some typical micro-tripods with various cavities L = 6.5–15.0 μm. h) The lasing mode wavelengths of $CdS_{0.48}Se_{0.52}$ micro-tripods as a function for the corresponding size-dependent cavities in (g).

purge the oxygen from the tube. Second, the N_2 flow was increased to 115 sccm, while the pressure in the tube was maintained at 225 Torr. Then, the furnace was heated to 800 °C at a rate of 27 °C min^{-1}, and the growth time was 60 min. Lastly, the furnace was decreased to room temperature naturally. In addition, ZnS and CdSSe alloy micro-tripods were prepared through the same method, while the growth pressure of ZnS tripods was maintained at 50 Torr, and the growth temperature was heated to 1000 °C at a rate of 17 °C min^{-1}. The growth pressure of CdSSe alloy micro-tripods was 205 Torr, with a growth temperature of ≈800 °C.

Characterization: The morphology of these micro-structures was investigated by SEM (Hitachi, S-4800, Japan) with EDX. The crystal structure was measured by X-ray diffraction (XRD, Bruker D8). The crystal structures were determined by transmission electron microscopy (TEM, JEM-F200). A self-made confocal optical system was used to test the optical properties of the micro-tripods, PL spectra, and 2D PL mapping. A laser beam (375 nm) was focused to a spot size of ≈0.5 μm by a microscope lens (Nikon, ×100) and locally excited at the structures. The PL spectra were recorded by an Ocean Optics Spectrometer (Maya Pro2000), and real color images were recorded by a CCD camera. Stimulated emission properties were studied using a 355 nm pulse laser focused at 100 μm. The micro-tripods were selected and transferred to a Si substrate by a 3D manipulator with self-made fiber probes for characterization.

Supporting Information

Supporting Information is available from the Wiley Online Library or from the author.

Acknowledgements

S.X., X.Z., and G.B. contributed equally to this work. The authors are grateful to the National Natural Science Foundation of China (no. 52373246), the Fundamental Research Program of Shanxi Provinces (no. 20210302123128 and 20210302123221), and the Graduate Education Innovation Program from Shanxi Provincial (no.2022Y271) for financial support.

Conflict of Interest

The authors declare no conflict of interest.

Data Availability Statement

The data that support the findings of this study are available from the corresponding author upon reasonable request.

Keywords

composition tunable, micro-tripods, mode-tunable lasers, nanophotonics, red–green–blue emissions

Received: February 21, 2024
Revised: March 17, 2024
Published online: March 30, 2024

[1] F. Fan, S. Turkdogan, Z. Liu, D. Shelhammer, C. Z. Ning, *Nat. Nanotechnol.* **2015**, *10*, 796.
[2] C. Ning, L. Dou, P. Yang, *Nat. Rev. Mater.* **2017**, *2*, 17070.
[3] P. Guo, X. Zhuang, J. Xu, Q. Zhang, W. Hu, X. Zhu, X. Wang, Q. Wan, P. He, H. Zhou, A. Pan, *Nano Lett.* **2013**, *13*, 1251.
[4] L. Dou, M. Lai, C. S. Kley, Y. Yang, C. G. Bischak, D. Zhang, S. W. Eaton, N. S. Ginsberg, P. Yang, *Proc. Natl. Acad. Sci. USA* **2017**, *114*, 7216.
[5] L. N. Quan, J. Kang, C. Ning, P. Yang, *Chem. Rev.* **2019**, *119*, 9153.
[6] Z. Yang, J. Xu, P. Wang, X. Zhuang, A. Pan, L. Tong, *Nano Lett.* **2011**, *11*, 5085.
[7] M. García-Tecedor, J. Bartolomé, D. Maestre, A. Trampert, A. Cremades, *Nano Res.* **2019**, *12*, 441.
[8] P. M. Lewis, D. Hebbar, N. K. S. Choudhari, S. D. Kulkarni, *Mater. Sci. Semicond. Process.* **2022**, *138*, 106284.
[9] E. F. Schubert, J. K. Kim, *Science* **2005**, *308*, 1274.
[10] G. Cossu, A. M. Khalid, P. Choudhury, R. Corsini, E. Ciaramella, *Opt. Express* **2012**, *20*, 501.
[11] K. Seo, T. Lim, S. Kim, H. L. Park, S. Ju, *Nanotechnology* **2010**, *21*, 255201.
[12] H. P. T. Nguyen, S. Zhang, K. Cui, X. Han, S. Fathololoumi, M. Couillard, G. A. Botton, Z. Mi, *Nano Lett.* **2011**, *11*, 1919.
[13] H. Lin, Y. Lu, H. Chen, H. Lee, S. Gwo, *Appl. Phys. Lett.* **2010**, *97*, 73101.
[14] Y. Ding, Q. Yang, X. Guo, S. Wang, F. Gu, J. Fu, Q. Wan, J. Cheng, L. Tong, *Opt. Express* **2009**, *17*, 21813.
[15] C. Zhang, L. Yang, J. Zhao, B. Liu, M. Y. Han, Z. Zhang, *Angew. Chem.* **2015**, *127*, 11693.
[16] S. Sapra, S. Mayilo, T. A. Klar, A. L. Rogach, J. Feldmann, *Adv. Mater.* **2007**, *19*, 569.
[17] X. Zhuang, P. Guo, Q. Zhang, H. Liu, D. Li, W. Hu, X. Zhu, H. Zhou, A. Pan, *Nano Res.* **2016**, *9*, 933.
[18] R. Mirhosseini, M. F. Schubert, S. Chhajed, J. Cho, J. K. Kim, E. F. Schubert, *Opt. Express* **2009**, *17*, 10806.
[19] M. H. Crawford, *IEEE J. Sel. Top. Quantum Electron* **2009**, *15*, 1028.
[20] Y. Ma, X. Guo, X. Wu, L. Dai, L. M. Tong, *Adv. Opt. Photonics* **2013**, *5*, 216.
[21] R. X. Yan, D. Gargas, P. D. Yang, *Nat. Photonics* **2009**, *3*, 569.
[22] Y. Lu, C. Wang, J. Kim, H. Chen, M. Lu, Y. Chen, W. Chang, L. Chen, M. I. Stockman, C. Shih, S. Gwo, *Nano Lett.* **2014**, *14*, 4381.
[23] E. Shi, B. Yuan, S. B. Shiring, Y. Gao, Y. G. Akriti, C. Su, M. Lai, P. Yang, J. Kong, B. M. Savoie, Y. Yu, L. Dou, *Nature* **2020**, *580*, 614.
[24] P. Guo, D. Liu, X. Shen, Q. Lv, Y. Wu, Q. Yang, P. Li, Y. Hao, J. C. Ho, K. M. Yu, *Nano Energy* **2022**, *92*, 106778.
[25] Q. Zhang, R. Su, X. Liu, J. Xing, T. C. Sum, Q. Xiong, *Adv. Funct. Mater.* **2016**, *26*, 6238.
[26] Z. Y. Yang, T. Albrow-Owen, H. X. Cui, J. Alexander-Webber, F. X. Gu, X. M. Wang, T. C. Wu, M. H. Zhuge, C. Williams, P. Wang, A. V. Zayats, W. W. Cai, L. Dai, S. Hofmann, M. Overend, L. M. Tong, Q. Yang, Z. P. Sun, T. Hasan, *Science* **2019**, *365*, 1017.
[27] J. Kim, C. Jo, M. G. Kim, G. S. Park, T. J. Marks, A. Facchetti, S. K. Park, *Adv. Mater.* **2022**, *34*, 2106215.
[28] B. Z. Tian, T. J. Kempa, C. M. Lieber, *Chem. Soc. Rev.* **2009**, *38*, 16.
[29] Q. Zhang, Q. Shang, R. Su, T. T. H. Do, Q. Xiong, *Nano Lett.* **2021**, *21*, 1903.
[30] P. Guo, M. K. Hossain, X. Shen, H. Sun, W. Yang, C. Liu, C. Y. Ho, C. K. Kwok, S. W. Tsang, Y. Luo, J. C. Ho, K. M. Yu, *Adv. Opt. Mater.* **2018**, *6*, 1801664.
[31] Y. Fu, H. Zhu, C. C. Stoumpos, Q. Ding, J. Wang, M. G. Kanatzidis, X. Zhu, S. Jin, *ACS Nano* **2016**, *10*, 7963.
[32] Z. Yang, D. Wang, C. Meng, Z. Wu, Y. Wang, Y. Ma, L. Dai, X. Liu, T. Hasan, X. Liu, Q. Yang, *Nano Lett.* **2014**, *14*, 3153.
[33] A. Pan, R. Liu, M. Sun, C. Ning, *ACS Nano* **2010**, *4*, 671.
[34] J. Xu, L. Ma, P. Guo, X. Zhuang, X. Zhu, W. Hu, X. Duan, A. Pan, *J. Am. Chem. Soc.* **2012**, *134*, 12394.
[35] T. Kuykendall, P. Ulrich, S. Aloni, P. Yang, *Nat. Mater.* **2007**, *6*, 951.
[36] P. L. Nichols, Z. Liu, L. Yin, S. Turkdogan, F. Fan, C. Z. Ning, *Nano Lett.* **2015**, *15*, 909.
[37] J. Li, C. Meng, Y. Liu, X. Wu, Y. Lu, Y. Ye, L. Dai, L. Tong, X. Liu, Q. Yang, *Adv. Mater.* **2013**, *25*, 833.
[38] X. Liu, Q. Zhang, Q. Xiong, T. C. Sum, *Nano Lett.* **2013**, *13*, 1080.
[39] H. Zhu, Y. Fu, F. Meng, X. Wu, Z. Gong, Q. Ding, M. V. Gustafsson, M. T. Trinh, S. Jin, X. Y. Zhu, *Nat. Mater.* **2015**, *14*, 636.
[40] M. Shoaib, X. Wang, X. Zhang, Q. Zhang, A. Pan, *Nano-Micro Lett.* **2018**, *10*, 58.
[41] J. Pan, M. I. B. Utama, Q. Zhang, X. Liu, B. Peng, L. M. Wong, T. C. Sum, S. Wang, Q. Xiong, *Adv. Mater.* **2012**, *24*, 4151.
[42] Y. Zhang, D. Lu, M. Gao, M. Lai, J. Lin, T. Lei, Z. Lin, L. N. Quan, P. Yang, *Proc. Natl. Acad. Sci. USA* **2019**, *116*, 12648.
[43] J. Xu, X. Zhuang, P. Guo, Q. Zhang, L. Ma, X. Wang, X. Zhu, A. Pan, *J. Mater. Chem. C* **2013**, *1*, 4391.
[44] D. J. Sirbuly, M. Law, P. Pauzauskie, H. Yan, A. V. Maslov, K. Knutsen, C. Z. Ning, R. J. Saykally, P. Yang, *Proc. Natl. Acad. Sci. USA* **2005**, *102*, 7800.
[45] S. Ullah, M. Zhuge, L. Zhang, X. Fu, Y. Ma, *Nanotechnology* **2024**, *35*, 205201.
[46] Q. Zhang, Y. Zhu, P. Niu, C. Lao, Y. Yao, W. Liu, Q. Yang, S. Chu, Y. Gao, *ACS Photonics* **2023**, *10*, 1397.
[47] W. Chen, L. Wang, R. Liu, H. Shen, J. Du, F. Fan, *Nano Lett.* **2023**, *23*, 437.
[48] S. Yang, X. Lu, J. Zhang, H. Wang, L. Sun, *Appl. Phys. Lett.* **2021**, *118*, 171101.
[49] J. Lim, Y. Park, V. I. Klimov, L. A. N. U. Los, *Nat. Mater.* **2018**, *17*, 42.
[50] Z. Liu, L. Yin, H. Ning, Z. Yang, L. Tong, C. Ning, *Nano Lett.* **2013**, *13*, 4945.
[51] T. K. Kormilina, S. A. Cherevkov, A. V. Fedorov, A. V. Baranov, *Small* **2017**, *13*, 1702300.
[52] A. Pan, W. Zhou, E. S. P. Leong, R. Liu, A. H. Chin, B. Zou, C. Z. Ning, *Nano Lett.* **2009**, *9*, 784.
[53] W. W. Wong, Z. Su, N. Wang, C. Jagadish, H. H. Tan, *Nano Lett.* **2021**, *21*, 5681.
[54] H. Sumikura, G. Zhang, M. Takiguchi, N. Takemura, A. Shinya, H. Gotoh, M. Notomi, *Nano Lett.* **2019**, *19*, 8059.
[55] G. Zhang, M. Takiguchi, K. Tateno, T. Tawara, M. Notomi, H. Gotoh, *Sci. Adv.* **2019**, *5*, 8896.
[56] X. Yan, W. Wei, F. Tang, X. Wang, L. Li, X. Zhang, X. Ren, *Appl. Phys. Lett.* **2017**, *110*, 061104.
[57] D. Saxena, N. Jiang, X. Yuan, S. Mokkapati, Y. Guo, H. H. Tan, C. Jagadish, *Nano Lett.* **2016**, *16*, 5080.
[58] X. Zhuang, Y. Ouyang, X. Wang, A. Pan, *Adv. Opt. Mater.* **2019**, *7*, 1900071.
[59] S. Chang, W. Liao, Y. Liao, H. Lin, H. Lin, W. Lin, S. Lin, P. Perumal, G. Haider, C. Tai, K. Shen, C. Chang, Y. Huang, T. Lin, Y. Chen, *Sci Rep.* **2018**, *8*, 2720.
[60] S. Chen, X. Zhao, Y. Wang, J. Shi, D. Liu, *Appl. Phys. Lett.* **2012**, *101*, 123508.

[61] G. Haider, H. Lin, K. Yadav, K. Shen, Y. Liao, H. Hu, P. K. Roy, K. P. Bera, K. Lin, H. Lee, Y. Chen, F. Chen, Y. Chen, *ACS Nano* **2018**, *12*, 11847.
[62] Q. W. Zhang, D. Li, X. Li, P. B. White, J. Mecinovic, X. Ma, H. Agren, R. J. M. Nolte, H. Tian, *J. Am. Chem. Soc.* **2016**, *138*, 13541.
[63] T. Zhai, Y. Wang, L. Chen, X. Wu, S. Li, X. Zhang, *Nanoscale* **2015**, *7*, 19935.
[64] T. Siegle, S. Schierle, S. Kraemmer, B. Richter, S. F. Wondimu, P. Schuch, C. Koos, H. Kalt, *Light Sci. Appl.* **2017**, *6*, 16224.
[65] X. Fang, T. Zhai, U. K. Gautam, L. Li, L. Wu, Y. Bando, D. Golberg, *Prog. Mater. Sci.* **2011**, *56*, 175.
[66] Q. Xiong, G. Chen, J. D. Acord, X. Liu, J. J. Zengel, H. R. Gutierrez, J. M. Redwing, L. C. Lew Yan Voon, B. Lassen, P. C. Eklund, *Nano Lett.* **2004**, *4*, 1663.